

Electronic Supplementary Information

Experimental section

Materials: Potassium hydroxide (KOH), potassium nitrate (KNO₃), copper (II) sulfate pentahydrate (CuSO₄·5H₂O), nickel sulfate hexahydrate (NiSO₄·6H₂O), potassium sulphate (K₂SO₄), potassium carbonate (K₂CO₃), potassium chloride (KCl), potassium hydrogen phosphate (K₂HPO₄) were purchased from Chengdu Kelong Chemical Reagent Co., Ltd. Sodium citrate dihydrate (C₆H₅Na₃O₇·2H₂O) was purchased from Aladdin Ltd. (Shanghai, China). Ti mesh was provided by Suzhou Taili New Energy Co., Ltd and treated with 1 M hydrochloric acid (HCl), ethanol, and ultrapure water for 10 minutes, respectively. All chemicals were used as received without further purification.

Preparation of CuNi/TM-20: Electrodeposited method was performed to synthesis CuNi/TM-20. Specifically, 2.6285 g NiSO₄·6H₂O, 2.941 g C₆H₅Na₃O₇·2H₂O, and 0.062 g CuSO₄·5H₂O were firstly dissolved in 50 ml ultrapure water to stir for 0.5 h to form an aqueous solution. After that, the electrodeposited method was conducted in an aqueous solution at a constant potential of -0.8 V vs. Ag/AgCl for 20 minutes, by using a treated Ti mesh, Ag/AgCl electrode, and Platinum (Pt) electrode as the working electrode, reference electrode, and counter electrode, respectively. Then, the resulting CuNi/TM-20 was washed by ultrapure water and dried in oven for an hour. The CuNi/TM-10 and CuNi/TM-30 samples were prepared by the same procedure but changing the electrodeposited time into 10 minutes and 30 minutes, respectively. Cu/TM-20 and Ni/TM-20 were fabricated using the same methods without NiSO₄·6H₂O and CuSO₄·5H₂O, respectively.

Characterizations: The crystal structures of the as-prepared materials were acquired by employing an X-ray diffractometer with a Cu K α radiation (40 kV, 30 mA) of wavelength 0.154 nm (SHIMADZU, Japan). The morphology information of the samples was unveiled by the scanning electron microscopy (SEM) measurement. The SEM images were obtained from a GeminiSEM 300 scanning electron microscope (ZEISS, Germany) at an accelerating voltage of 5 kV. An X-ray photoelectron spectrum (XPS, Esalab 250Xi) was utilized to probe into the chemical states of the samples. Gas chromatography (GC-2014C, SHIMADZU) was utilized to quantitatively detect H₂ and N₂. ¹H NMR spectra were collected on Varian VNMRS 600 MHz (USA).

Electrochemical measurements: All the electrochemical measurements were carried out in an H-shaped electrochemical cell separated by a treated Nafion 117 membrane using CHI 760E electrochemical workstation (Chenhua, Shanghai). The electrolyte solution (50 mL) was Ar-saturated 0.1 M KOH with and without 0.1 M NO₃⁻, where CuNi/TM-20, Hg/HgO electrode, and a graphite rod were used as working electrode, reference electrode, and counter electrode, respectively. The simulated wastewater was prepared by adding 0.01 M K₂SO₄, K₂CO₃, KCl and K₂HPO₄ into 0.1 M KOH solution. The area of the working electrode immersed in the electrolyte is 1 cm². The linear sweep voltammetry (LSV) curves were recorded by CHI 760E scans from 0.6 to -0.1 V at a scan rate of 10 mV s⁻¹. All potentials reported in this work were converted to a reversible hydrogen electrode (RHE) scale by using the following equation: E (RHE) = E (Hg/HgO) + (0.098 + 0.0591 × pH) V. And the current densities were normalized to the geometric surface area. All experiments were carried out at room temperature (25 °C).

Determination of NH₃: The as-generated NH₃ was quantitatively determined via a spectrophotometry measurement using the indophenol blue method (the obtained electrolyte was diluted 40 times).¹ In detail, 2 mL of the diluted catholyte was obtained from the cathodic chamber and mixed with 2 mL of a 1 M NaOH solution that contained salicylic acid and sodium citrate. Then, 1 mL of 0.05 M NaClO and 0.2 mL of 1 wt% C₅FeN₆Na₂O were dropped into the collected electrolyte solution. After standing at room temperature for 2 h, the ultraviolet-visible absorption spectrum was measured. The concentration-absorbance curve was calibrated using the standard NH₄Cl solution with NH₃ concentrations of 0, 0.2, 0.4, 0.8, 1.0, 2.0 and 4.0 ppm in 0.1 M KOH. The absorbance at 655 nm was measured to quantify the NH₃ concentration using standard NH₄Cl solutions ($y = 0.3756 x + 0.0097$, $R^2 = 0.9998$).

Determination of NO₂⁻: The NO₂⁻ concentration was measured by Griess reagent using UV spectrophotometry.² The Griess reagent was prepared by dissolving 0.1 g N-(1-naphthyl) ethylenediamine dihydrochloride, 1.0 g sulfonamide, and 2.94 mL H₃PO₄ in 50 mL deionized water. Typically, 1.0 mL Griess reagent was mixed with 1.0 mL electrolyte and 2.0 mL H₂O. After reacting at room temperature for 10 min, the absorbance at 540 nm was measured to quantify the NO₂⁻ concentration with a standard curve of NO₂⁻ ($y = 0.20714 x + 0.04733$, $R^2 = 0.9998$).

Determination of N₂H₄: The concentration of the electrogenerated N₂H₄ was assessed by Watt and Chrisp's method.³ The chromogenic reagent was a mixed solution of 5.99 g C₉H₁₁NO, 30 mL HCl and 300 mL C₂H₅OH. In detail, 1 mL of electrolyte was added into 1 mL prepared colour reagent and stirred for 15 min in the dark. The absorbance at 455 nm was measured to quantify the N₂H₄ concentration by dint of standard N₂H₄ solutions. ($y = 0.7798 x + 0.03416$, $R^2 = 0.999$).

Calculations of FE and NH₃ yield:

The amount of NH₃ (m_{NH3}) was calculated by the following equation:

$$m_{\text{NH}_3} = [\text{NH}_3] \times V$$

FE of NH₃ formation was calculated by the following equation:

$$\text{FE} = (n \times F \times [\text{NH}_3] \times V) / (M_{\text{NH}_3} \times Q) \times 100\%$$

The NH₃ yield rate is calculated using the following equation:

$$\text{NH}_3 \text{ yield} = ([\text{NH}_3] \times V) / (t \times A \times 17)$$

Where F is the Faradaic constant (96485 C mol⁻¹), n is the electrons transfer number (8 for NH₃), [NH₃] is the NH₃ concentration, V is the volume of electrolyte in the cathodic compartment (50 mL), M_{NH3} is the molar mass of the NH₃ molecule (17), Q is the total charge during electrosynthesis; t is the reduction time (1 h) and A is the geometric area of the working electrode (1 × 1 cm²).

¹⁵N isotopic labelling experiments: The generated NH₃ was demonstrated by an isotope-labelled tracer experiment using a 0.1 M ¹⁵NO₃⁻ as a N source. After 1 h electrolysis at -0.5 V, 2 mL electrolyte retrieved from the cathodic chamber was neutralized by 1.2 M HCl aqueous solution. After that, 500 ul of neutralized electrolyte was mixed with 50 ul deuterium oxide (D₂O). Then the mixture was then sealed into a nuclear magnetic resonance (NMR) tube (5 mm in diameter, 600 MHz) for further tests.

Calculation of the partial current density:

$$j_{\text{partial}} = \text{FE} \times I$$

Among them, j_{partial} represents the partial current density at each given potential; FE represents the calculated Faradaic efficiency of each product at each given potential; I represents the current density of each product at each given potential.

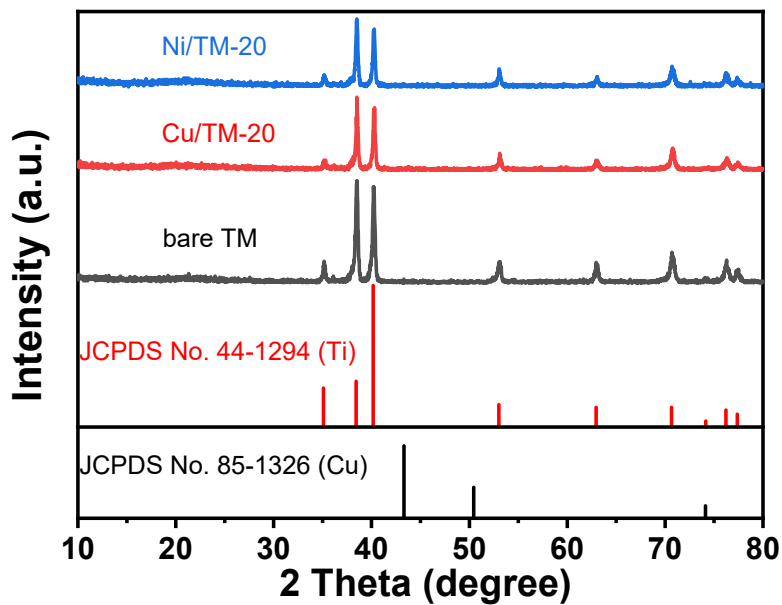


Fig. S1. XRD pattern of Ni/TM-20, Cu/TM-20, and bare TM.

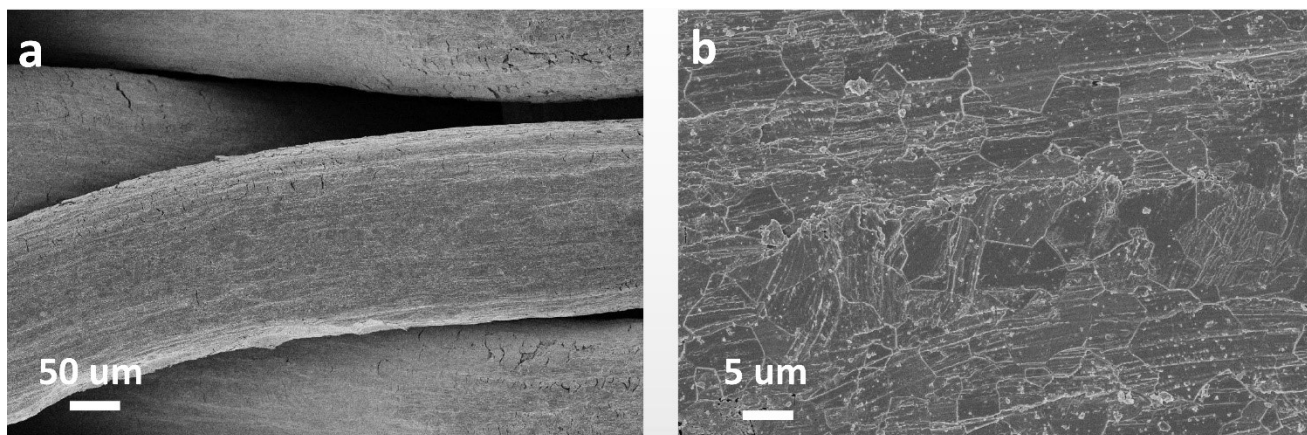


Fig. S2. SEM images for bare TM.

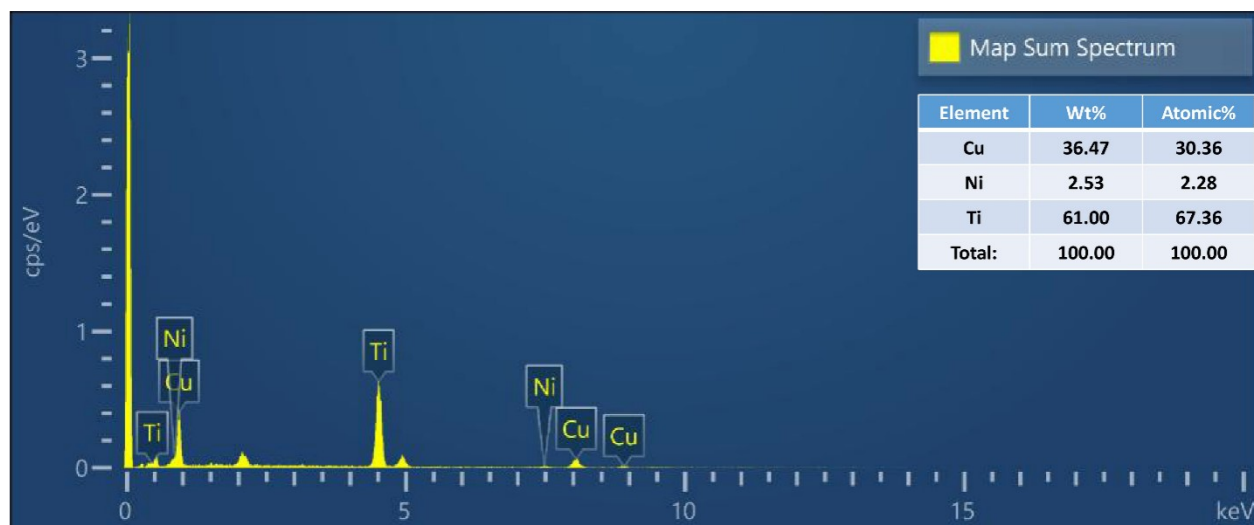


Fig. S3. Energy dispersive X-ray (EDX) spectra of CuNi/TM-20 catalyst.

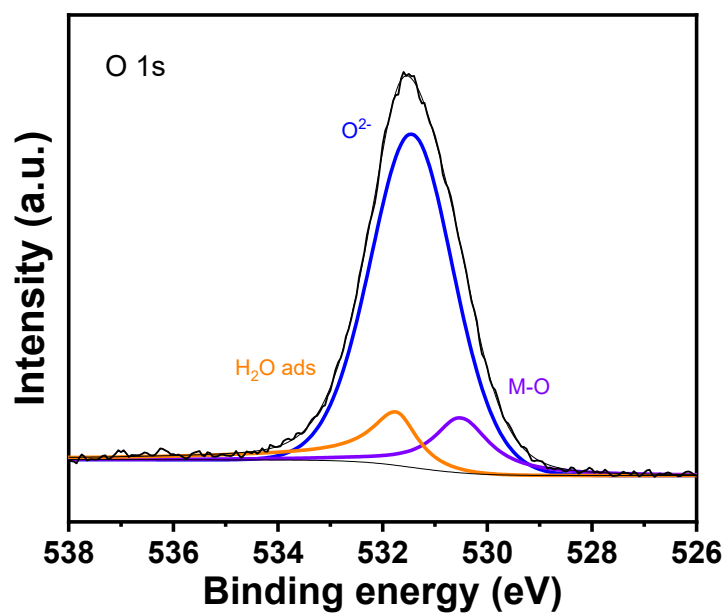


Fig. S4. XPS spectrum of CuNi/TM-20 in the O 1s region.

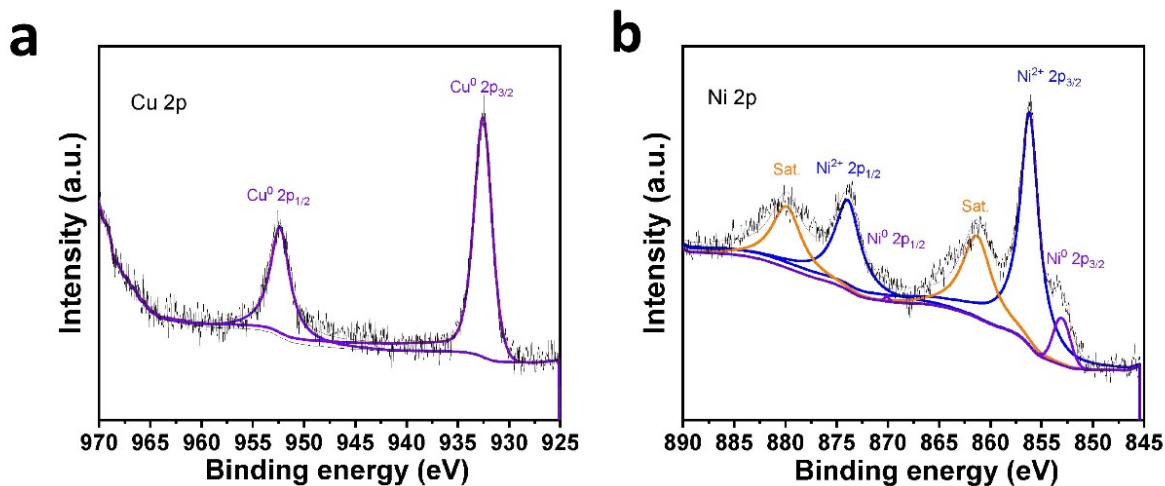


Fig. S5. XPS spectra of (a) Cu/TM-20 and (b) Ni/TM-20.

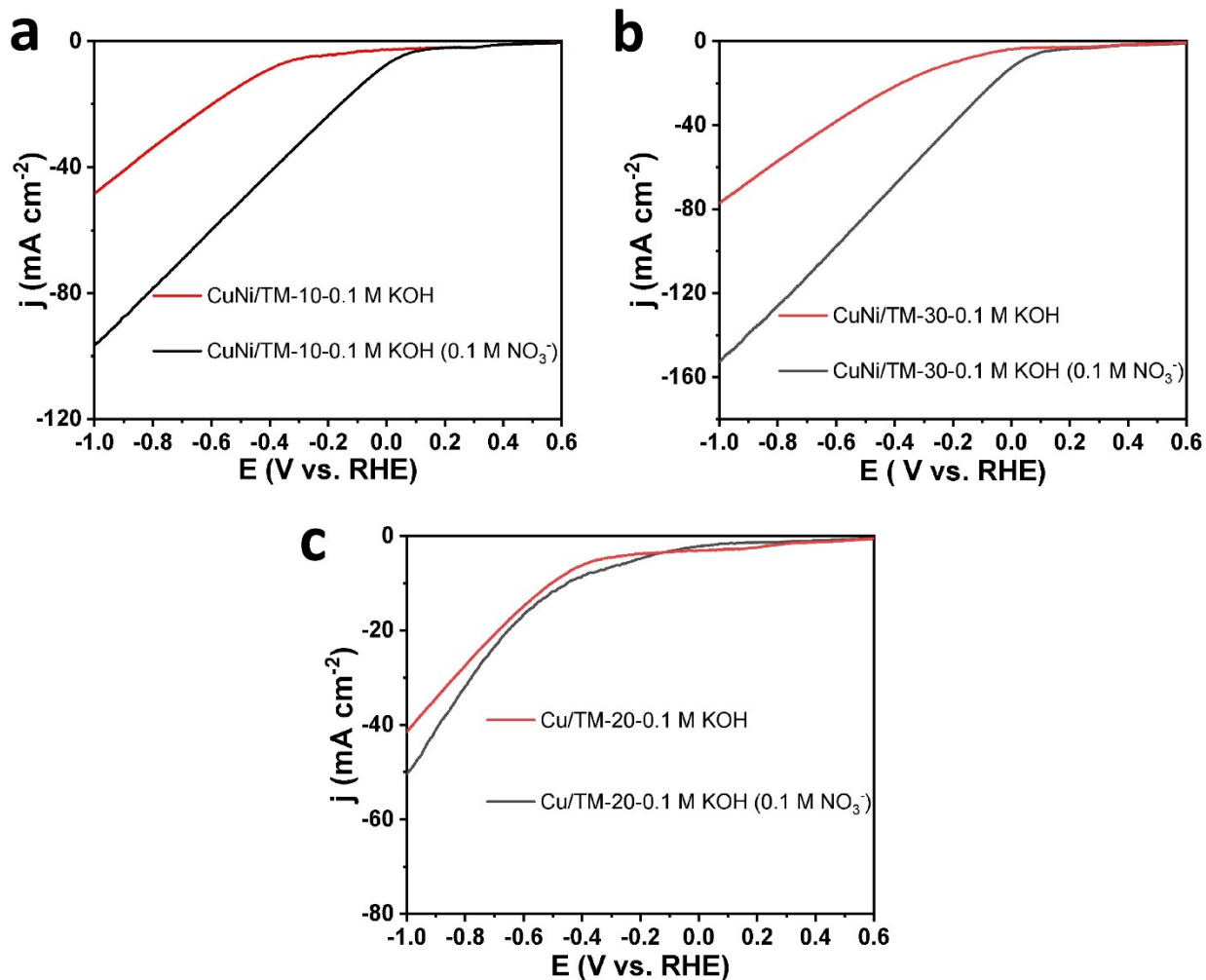


Fig. S6. LSV curves of (a) CuNi/TM-20, (b) CuNi/TM-30, and (c) Cu/TM-20 in 0.1 M KOH with and without 0.1 M NO₃⁻.

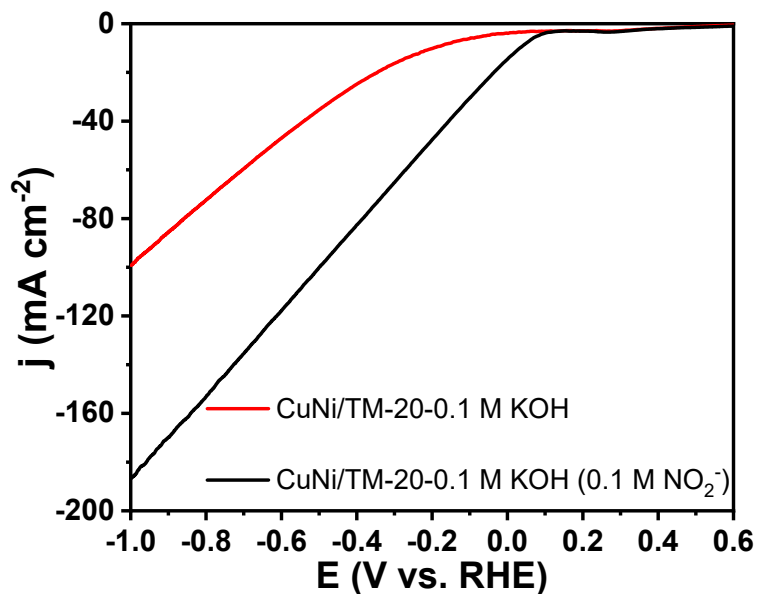


Fig. S7. LSV curves of CuNi/TM-20 in 0.1 M KOH with and without 0.1 M NO₂⁻.

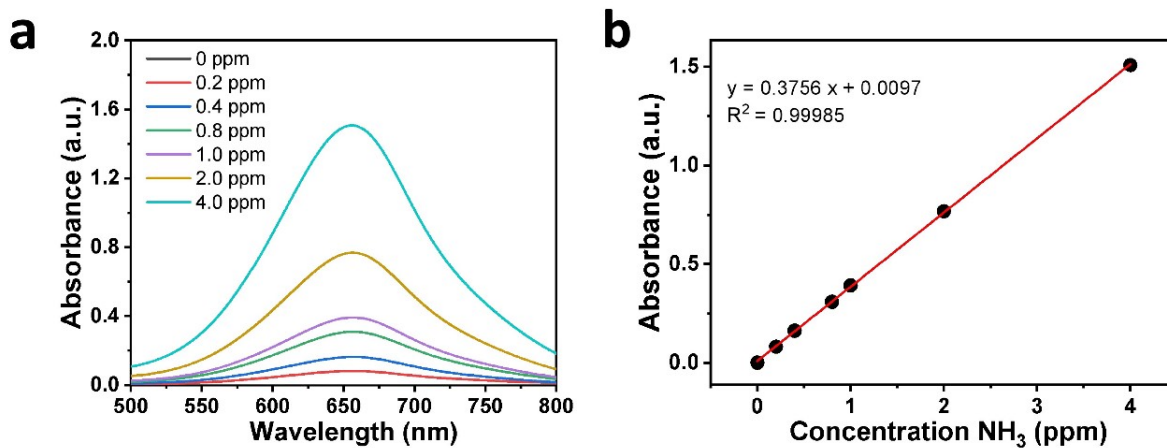


Fig. S8. (a) UV-Vis absorption spectra of indophenol assays kept with different concentrations of NH₃ after incubated for 2 h at room temperature. (b) Corresponding calibration curves used for calculation of NH₃ concentration.

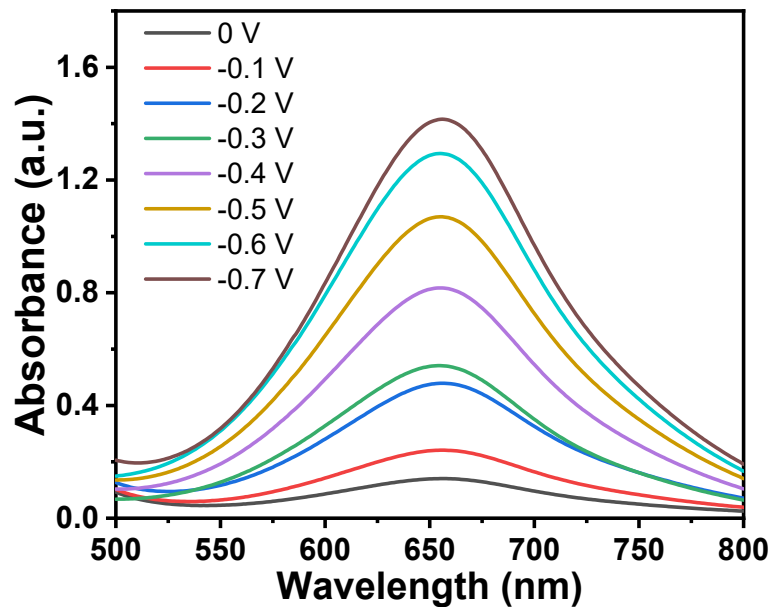


Fig. S9. UV-Vis absorption spectra of the electrolyte for calculating NH_3 concentration at each given potential.

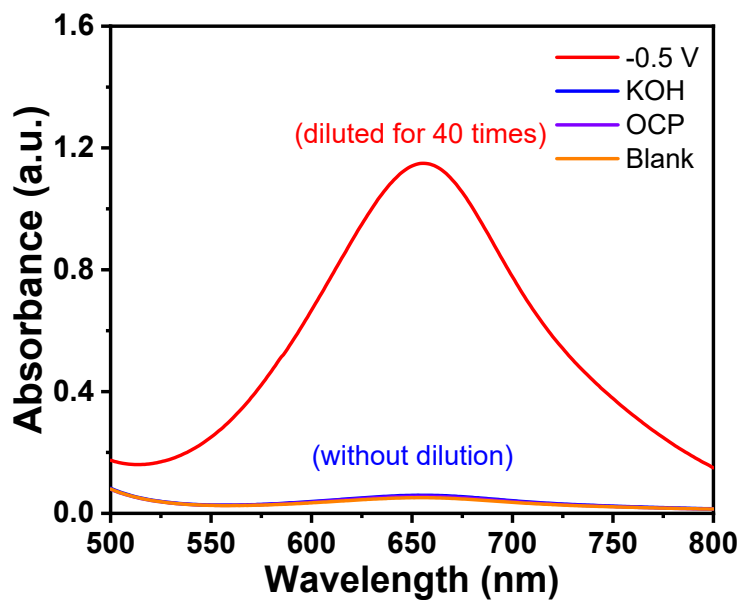


Fig. S10. UV-Vis absorption spectra of NH_3 concentrations at different conditions.

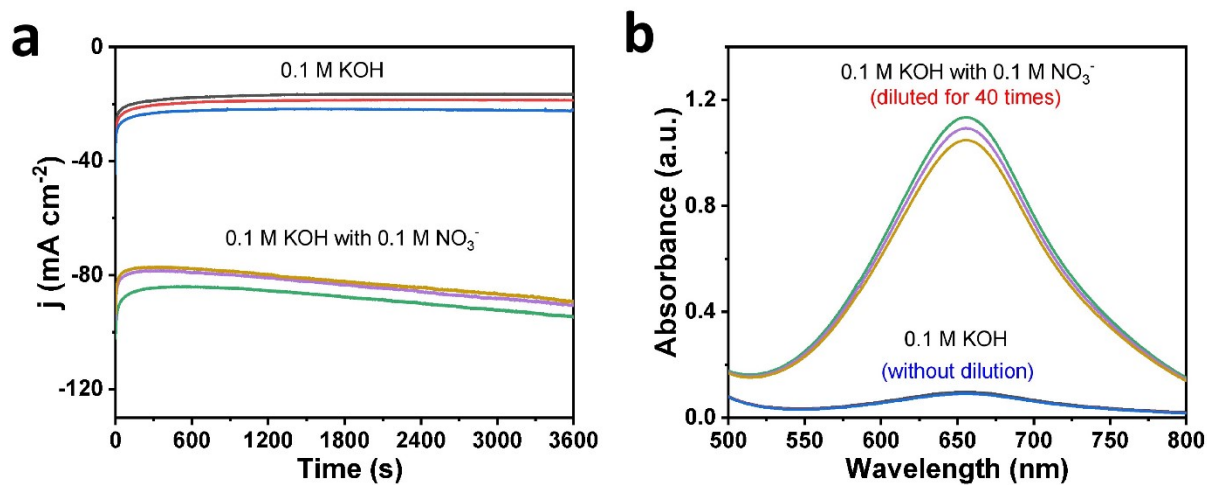


Fig. S11. (a) Chronoamperometry curves and (b) corresponding UV-vis adsorption spectra of CuNi/TM-20 for electrochemical catalytic production of NH₃ during the alternative experiments between NO₃⁻-containing and NO₃⁻-free 0.1 M KOH solution.

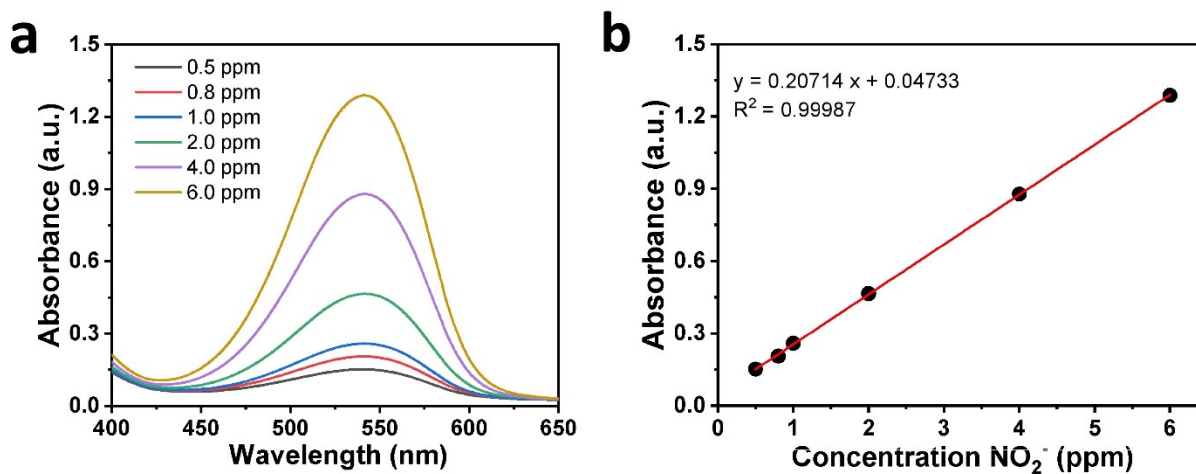


Fig. S12. (a) UV-Vis absorption spectra of different concentrations of NO₂⁻ after incubated for 10 min at room temperature. (b) Corresponding calibration curves used for calculation of NO₂⁻ concentration.

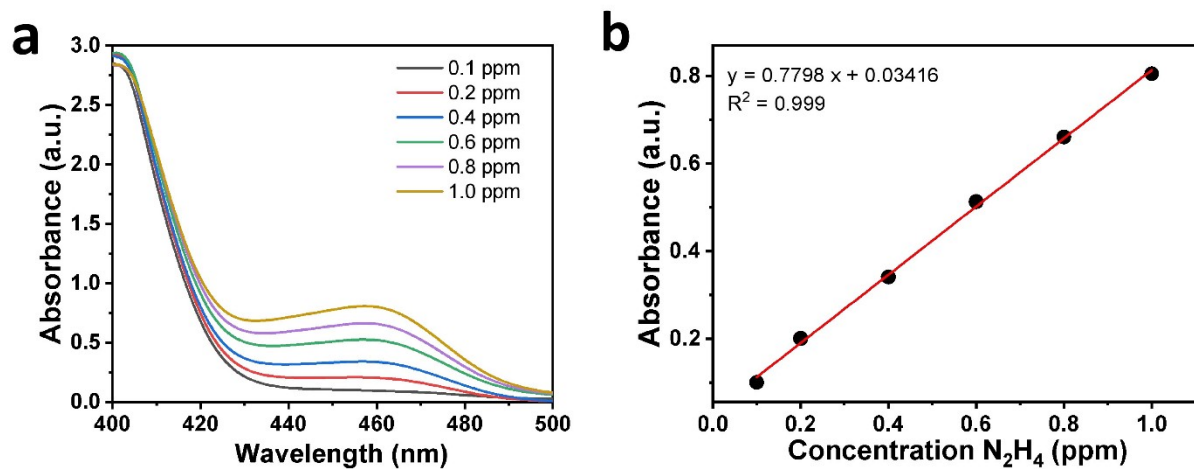


Fig. S13. (a) UV-Vis absorption spectra of different concentrations of N_2H_4 after incubated for 15 min at room temperature. (b) Corresponding calibration curves used for calculation of N_2H_4 concentration.

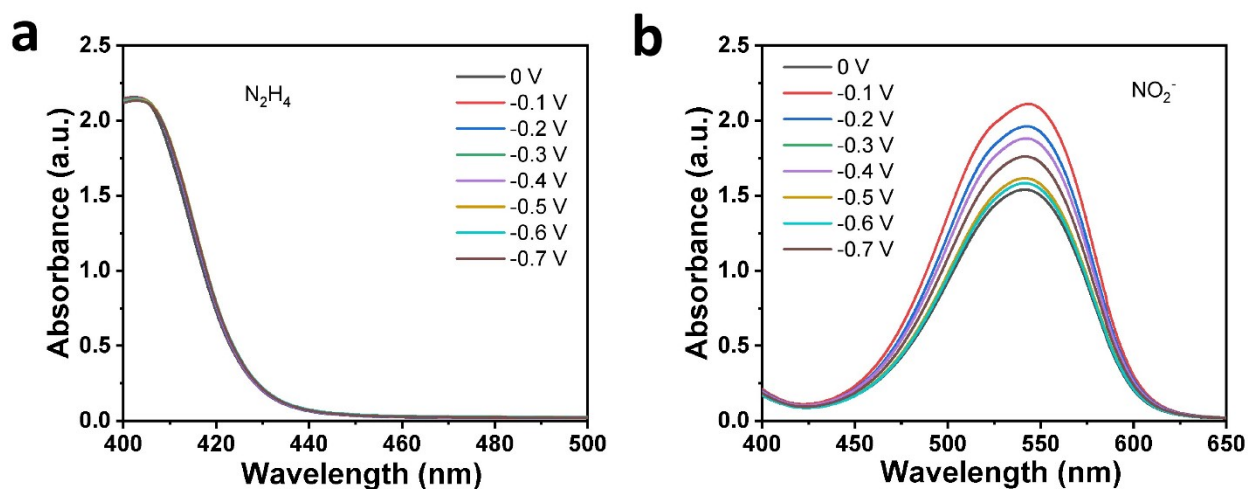


Fig. S14. UV-Vis absorption spectra of electrogenerated (a) N_2H_4 and (b) NO_2^- .

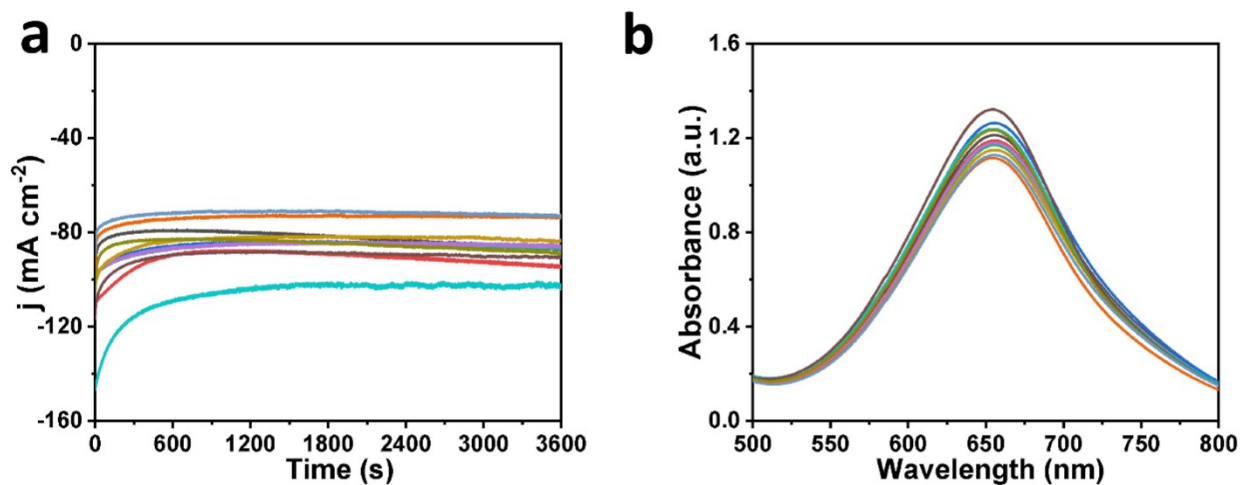


Fig. S15. (a) Chronoamperometry curves and (b) corresponding UV-vis adsorption spectra of CuNi/TM-20 for electrochemical catalytic production of NH_3 during cyclic tests at -0.5 V.

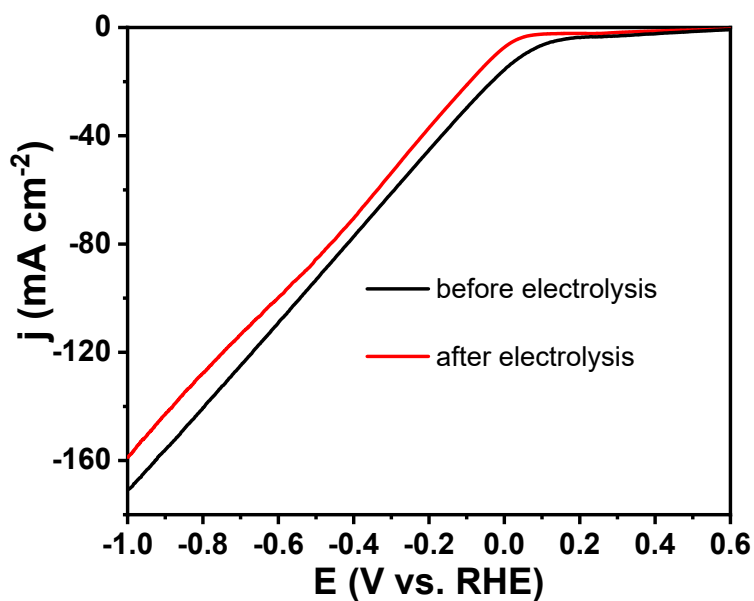


Fig. S16. LSV curves of CuNi/TM-20 before and after electrolysis.

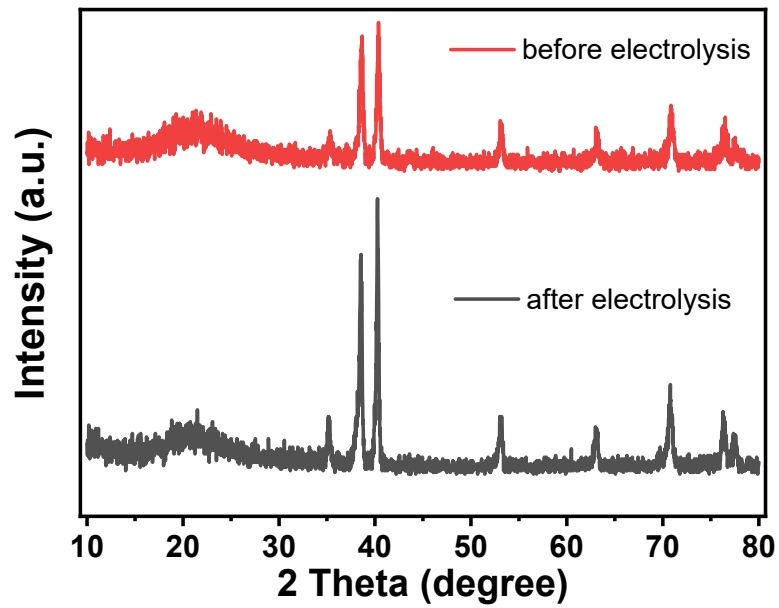


Fig. S17. XRD patterns of CuNi/TM-20 before and after electrolysis.

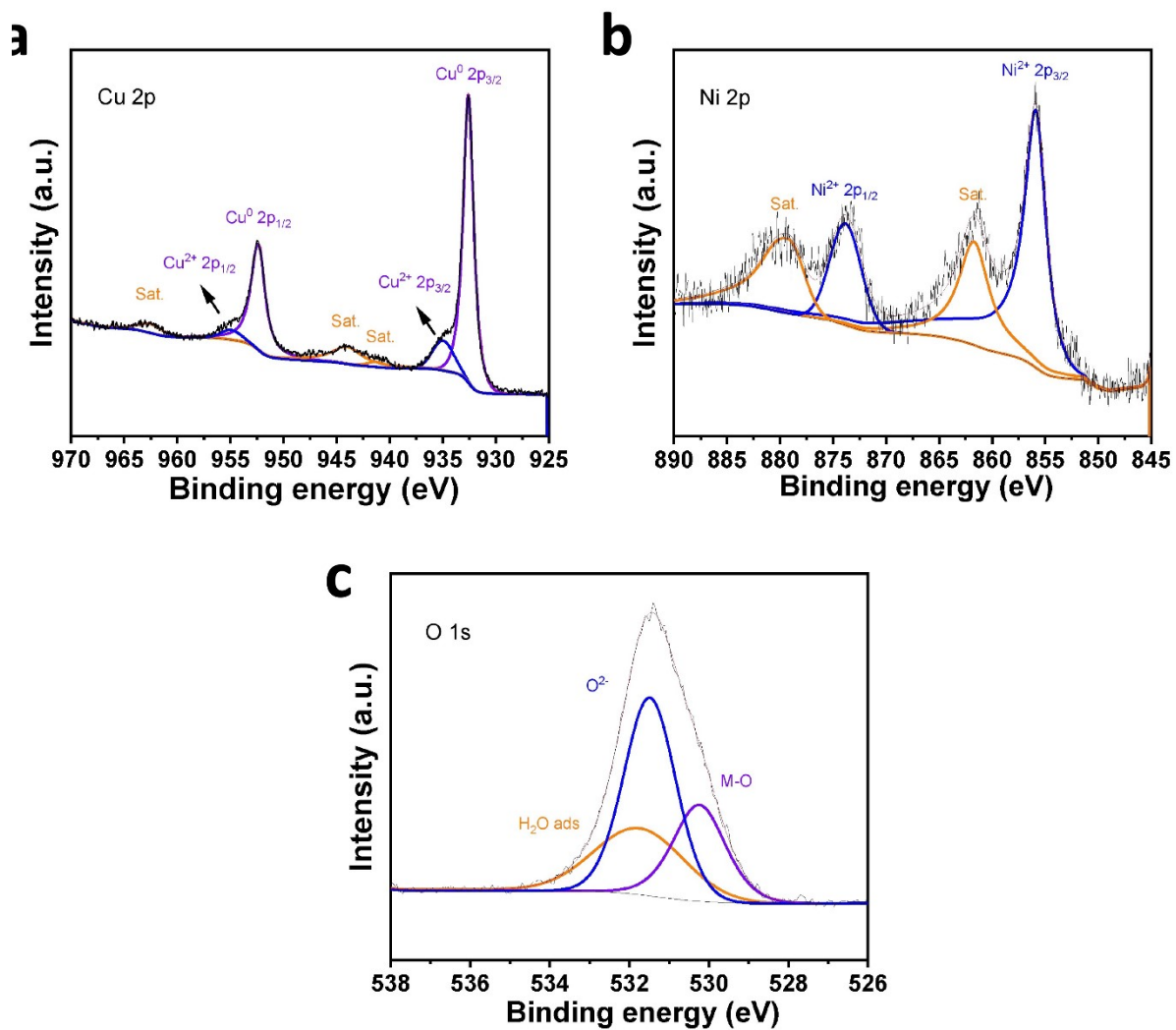


Fig. S18. XPS spectra of CuNi/TM-20 after electrolysis.

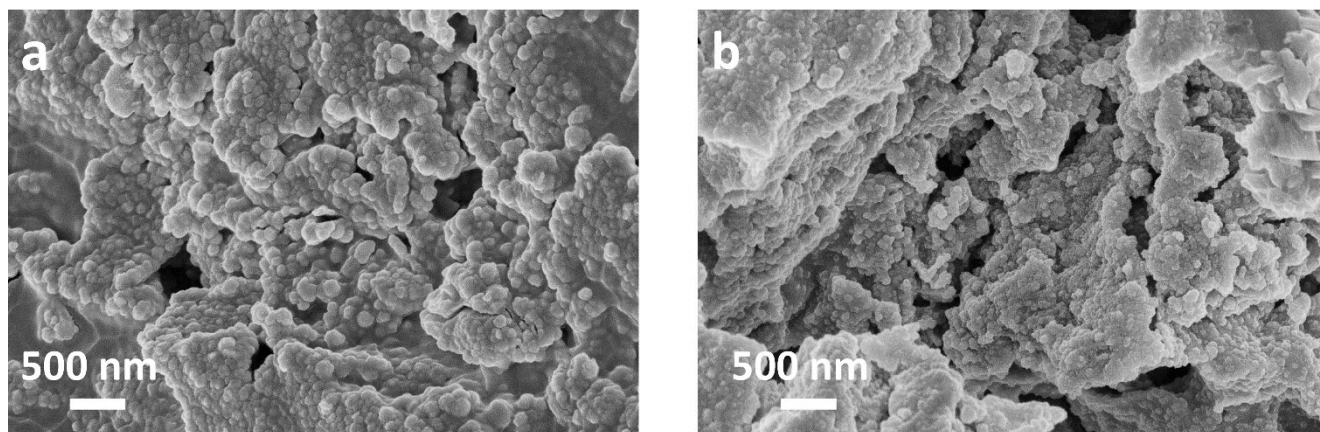


Fig. S19. SEM images of CuNi/TM-20 (a) before and (b) after electrolysis.

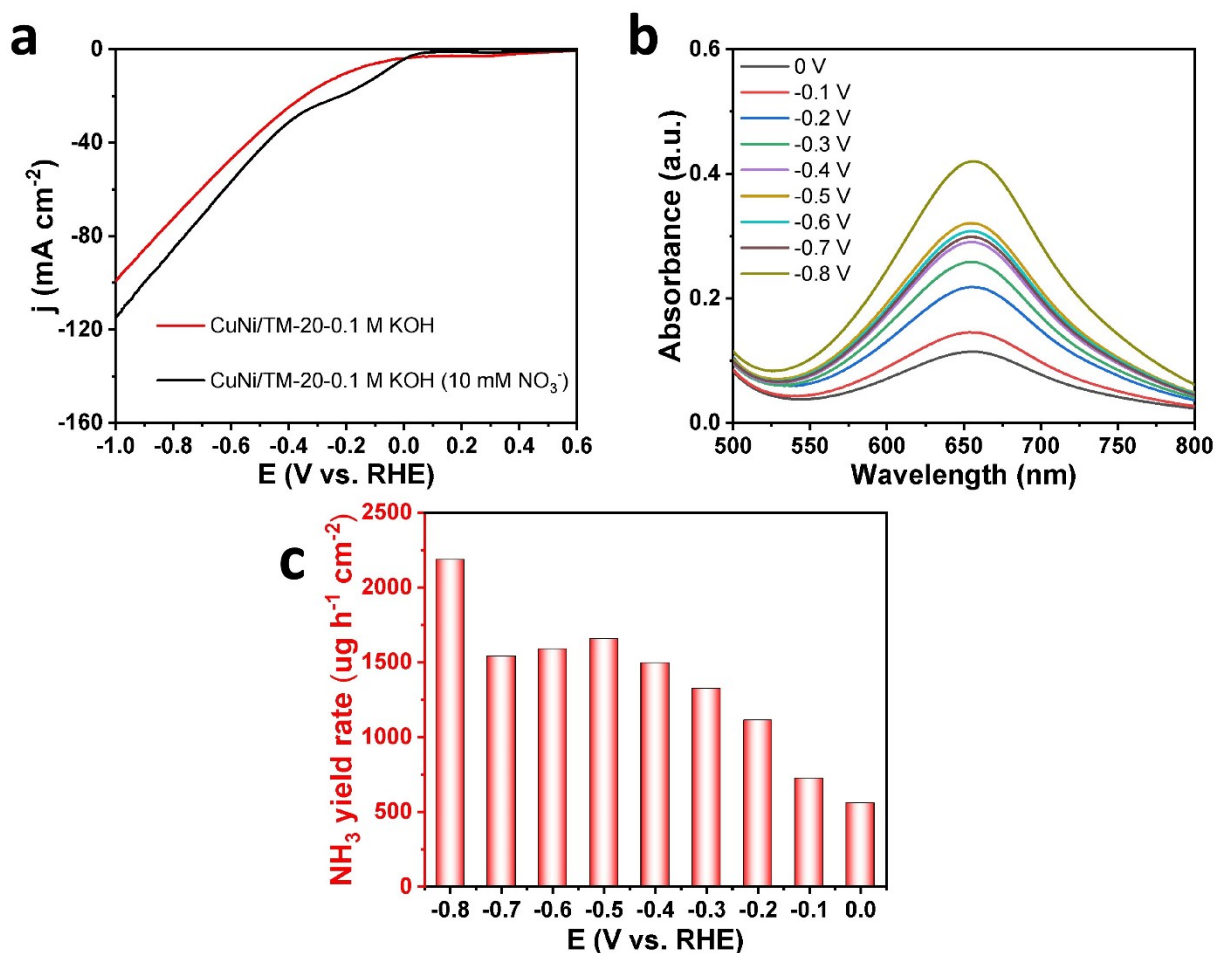


Fig. S20. (a) LSV curves of CuNi/TM-20 in 0.1 M KOH with and without 10 M NO₃⁻. (b) UV-vis adsorption spectra of CuNi/TM-20 for electrochemical catalytic production of NH₃ at each given potential. (c) Calculated NH₃ yield rates at each given potential.

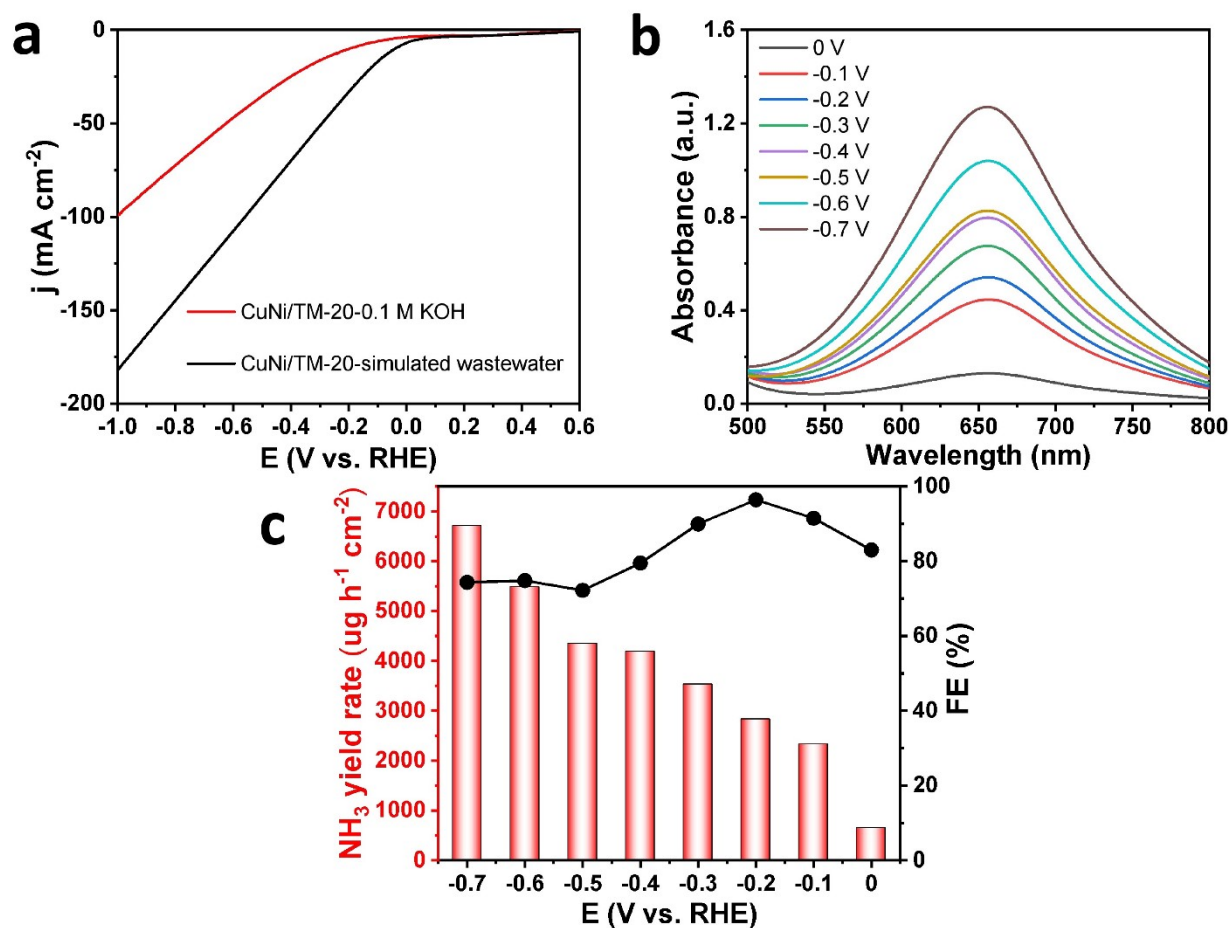


Fig. S21. (a) LSV curves of CuNi/TM-20 in 0.1 M KOH and simulated wastewater. (b) UV-vis adsorption spectra of CuNi/TM-20 for electrochemical catalytic production of NH₃ at each given potential. (c) Calculated NH₃ yield rates and FEs at each given potential.

Table S1. Comparing the catalytic performances of CuNi/TM-20 with other reported NO₃⁻RR electrocatalysts.

Catalyst	Electrolyte	Onset potential	Performance	Ref.
CuNi/TM-20	0.1 M KOH (0.1 M NO ₃ ⁻)	0 V vs. RHE	NH ₃ yield rate: 5644 ug h ⁻¹ cm ⁻² FE:93.1%	This work
Oxo-MoSx	0.1 M PBS (0.1 M NO ₃ ⁻)	/	NH ₃ yield rate: / FE: 96%	4
Cu ₃ P NA/CF	0.1 M PBS (0.1 M NO ₃ ⁻)	-0.5 V vs. RHE	NH ₃ yield rate: 848 ug h ⁻¹ cm ⁻² FE: 62.9%	5
BCN@Ni	0.1 M KOH (0.1 M NO ₃ ⁻)	-0.1 V vs. RHE	NH ₃ yield rate: 1904.2 ug h ⁻¹ cm ⁻² FE:68.17%	6
Fe-PPy SACs	0.1 M KOH (0.1 M NO ₃ ⁻)	0.2 V vs. RHE	NH ₃ yield rate: 2750 ug h ⁻¹ cm ⁻² FE: 100 %	7
Ni ₃ B@NiB _{2.74}	0.1 M KOH (0.1 M NO ₃ ⁻)	0.1 V vs. RHE	NH ₃ yield rate: 3371.1 ug h ⁻¹ cm ⁻² FE: 100%	8
TiO ₂ -x	0.5 M Na ₂ SO ₄ (50 ppm NO ₃ ⁻)	-1.4 V vs. RHE	NH ₃ yield rate: 850 ug h ⁻¹ cm ⁻² FE: 85%	9
PTCDA/O-Cu	0.1 M PBS (500 ppm NO ₃ ⁻)	-0.1 V vs. RHE	NH ₃ yield rate: 436±85 ug h ⁻¹ cm ⁻² FE: 85.9%	10
Cu nanosheets	0.1 M KOH (10 mM NO ₃ ⁻)	-0.5 V vs. RHE	NH ₃ yield rate: 390.1 ug h ⁻¹ cm ⁻² FE: 99.7%	11
Cu ₅₀ Ni ₅₀	0.1 M KOH (10 mM NO ₃ ⁻)	/	NH ₃ yield rate: / FE: 84±2%	12
Co ₃ O ₄ @NiO HNTs	3.28 mM Na ₂ SO ₄ (200 ppm NO ₃ ⁻)	-1.1 V vs. RHE	NH ₃ yield rate: 3305 ug h ⁻¹ cm ⁻² FE: 93.8%	13
PP-Co	0.1 M NaOH (0.1 M NO ₃ ⁻)	-0.3 V vs. RHE	NH ₃ yield rate: 1.1 mmol h ⁻¹ cm ⁻² FE: 90.1	14
FeOOH/CP	0.1 M PBS (0.1 M NO ₃ ⁻)	-0.4 V vs. RHE	NH ₃ yield rate: 2419 ug h ⁻¹ cm ⁻² FE: 92%	15
CFP-Cu ₁ Ni ₁	0.5 M Na ₂ SO ₄ (0.1 M NO ₃ ⁻)	-0.02 V vs. RHE	NH ₃ yield rate: 180 umol h ⁻¹ cm ⁻² FE: 95.7%	16

References

- 1 D. Zhu, L. Zhang, R. E. Ruther and R. J. Hamers, *Nat. Mater.*, 2013, **12**, 836–841.
- 2 L. C. Green, D. A. Wagner, J. Glogowski, P. L. Skipper, J. S. Wishnok and S. R. Tannenbaum, *Anal. Biochem.*, 1982, **126**, 131–138.
- 3 G. W. Watt and J. D. Chrisp, *Anal. Chem.*, 1952, **24**, 2006–2008.
- 4 Y. Li, Y. K. Go, H. Ooka, D. He, F. Jin, S. H. Kim and R. Nakamura, *Angew. Chem., Int. Ed.*, 2020, **59**, 9744–9750.
- 5 J. Liang, B. Deng, Q. Liu, G. Wen, Q. Liu, T. Li, Y. Luo, A. A. Alshehri, K. A. Alzahrani, D. Ma and X. Sun, *Green Chem.*, 2021, **23**, 5487–5493.
- 6 X. Zhao, Z. Zhu, Y. He, H. Zhang, X. Zhou, W. Hu, M. Li, S. Zhang, Y. Dong, X. Hu, A. V. Kuklin, G. V. Baryshnikov, H. Ågren, T. Wågberg and G. Hu, *Chem. Eng. J.*, 2022, **433**, 133190.
- 7 P. Li, Z. Jin, Z. Fang and G. Yu, *Energy Environ. Sci.*, 2021, **14**, 3522–3531.
- 8 L. Li, C. Tang, X. Cui, Y. Zheng, X. Wang, H. Xu, S. Zhang, T. Shao, K. Davey and S. Z. Qiao, *Angew. Chem., Int. Ed.*, 2021, **60**, 14131–14137.
- 9 R. Jia, Y. Wang, C. Wang, Y. Ling, Y. Yu and B. Zhang, *ACS Catal.*, 2020, **10**, 3533–3540.
- 10 G. F. Chen, Y. Yuan, H. Jiang, S. Y. Ren, L. X. Ding, L. Ma, T. Wu, J. Lu and H. Wang, *Nat. Energy*, 2020, **5**, 605–613.
- 11 X. Fu, X. Zhao, X. Hu, K. He, Y. Yu, T. Li, Q. Tu, X. Qian, Q. Yue, M. R. Wasielewski and Y. Kang, *Appl. Mater. Today*, 2020, **19**, 100620.
- 12 Y. Wang, A. Xu, Z. Wang, L. Huang, J. Li, F. Li, J. Wicks, M. Luo, D. H. Nam, C. S. Tan, Y. Ding, J. Wu, Y. Lum, C. T. Dinh, D. Sinton, G. Zheng and E. H. Sargent, *J. Am. Chem. Soc.*, 2020, **142**, 5702–5708.
- 13 Y. Yu, C. Wang, Y. Yu, Y. Wang and B. Zhang, *Sci. China Chem.*, 2020, **63**, 1469–1476.
- 14 Q. Chen, J. Liang, Q. Liu, K. Dong, L. Yue, P. Wei, Y. Luo, Q. Liu, N. Li, B. Tang, A. A. Alshehri, M. S. Hamdy, Z. Jiang and X. Sun, *Chem. Commun.*, 2022, **58**, 4259–4262.
- 15 Q. Liu, Q. Liu, L. Xie, Y. Ji, T. Li, B. Zhang, N. Li, B. Tang, Y. Liu, S. Gao, Y. Luo, L. Yu, Q. Kong and X. Sun, *ACS Appl. Mater. Interfaces*, 2022, **14**, 17312–17318.
- 16 Z. Zhang, Y. Liu, X. Su, Z. Zhao, Z. Mo, C. Wang, Y. Zhao, Y. Chen and S. Gao, *Nano Res.*, 2023, **16**, 6632–6641.